# CREBRF p.Arg457Gln Promotes Obesity and Improves Insulin Sensitivity by Promoting Preadipocyte Differentiation and Reducing Oxidative Metabolism in Gene-modified Pig Models

**Yingying Li**
Guangzhou Institutes of Biomedicine and Health, Chinese Academy of Sciences
**Hai Wang**
Guangzhou Institutes of Biomedicine and Health
**Yuan Liao**
Guangzhou Institutes of Biomedicine and Health
**Quanmei Yan**
Guangzhou Institutes of Biomedicine and Health
**Zhen Ouyang**
Guangzhou Institutes of Biomedicine and Health
**Yu Zhao**
Guangzhou Institutes of Biomedicine and Health
**Quanjun Zhang**
Guangzhou Institutes of Biomedicine and Health
**Chengdan Lai**
Guangzhou Institutes of Biomedicine and Health
**Zhaoming Liu**
Guangzhou Institutes of Biomedicine and Health
**Zhenpeng Zhuang**
Guangzhou Institutes of Biomedicine and Health
**Hao Li**
Guangzhou Institutes of Biomedicine and Health
**Shuwen Zheng**
Wuyi University
**Jiaowei Wang**
Guangzhou Institutes of Biomedicine and Health
**Chuan Li**
Guangzhou Institutes of Biomedicine and Health
**Yangyang Suo**
Guangzhou Institutes of Biomedicine and Health

**Ting Lan**
Guangzhou Institutes of Biomedicine and Health
**Yang Liu**
Guangzhou Institutes of Biomedicine and Health
**Yinghua Ye**
Guangzhou Institutes of Biomedicine and Health
**Qingjian Zou**
Guangzhou Institutes of Biomedicine and Health
**Zhen Dai**
Guangzhou Institutes of Biomedicine and Health
**Tao Nie**
Guangzhou Institutes of Biomedicine and Health
**Donghai Wu**
Guangzhou Institutes of Biomedicine and Health
**Nana Fan**
Guangzhou Institutes of Biomedicine and Health
**Liangxue Lai** ( lai_liangxue@gibh.ac.cn )
Guangzhou Institutes of Biomedicine and Health, Chinese Academy of Sciences

---

**Article**

**Keywords:** CREBRF, pig models, type 2 diabetes, obesity, oxidative metabolism

**Posted Date:** October 26th, 2021

**DOI:** https://doi.org/10.21203/rs.3.rs-970750/v1



---

# Abstract

Obesity is one of the most important risk factors for type 2 diabetes (T2DM). The *CREBRF* missense allele of rs373863828 (p.Arg457Gln) is associated with increased body mass index (BMI), yet reduced risk of T2DM in people with Pacific ancestry. To investigate the functional consequences of the CREBRF variant, we introduced the corresponding human mutation p.Arg457Gln into porcine genome by using a CRISPR/Cas9-mediated homologous recombination (HR)-dependent approach. The CREBRF p.Arg457Gln pig models displayed dramatically increased fat deposition, yet improved sensitivity to insulin. Transcriptome and metabolome analyses of subcutaneous white adipose tissues showed that the CREBRF p.Arg457Gln mutation promoted preadipocyte differentiation, which indicated that obesity was caused by increased number (hyperplasia) rather than size (hypertrophy) of adipocytes. In addition, the oxidative capacity decreased in the adipose tissue of pigs with CREBRF p.Arg457Gln variant. The pre-oxidative metabolite content (4-HNE and MDA) significantly decreased, while activity of antioxidant enzymes (GPX, SOD, and CAT) increased, thereby repressing oxidative metabolism of adipose tissue and reducing level of reactive oxygen species (ROS). The low reactive oxygen species could prevent insulin resistance and reduce risk of obesity-induced type 2 diabetes. This study provides further mechanistic insights into favourable adiposity resulting from *CREBRF* p.Arg457Gln.


# Introduction

Type 2 diabetes associated with insulin resistance and/or pancreatic beta cell dysfunction accounts for more than 90% of diabetes cases[1]. Many studies[2-5] have shown that obesity is one of the most important risk factors for type 2 diabetes. However, some people with obesity are metabolically healthy. The capacity of subcutaneous adipose tissue to expand and store excess lipids is thought to contribute to the variation in BMI among people who develop type 2 diabetes. Recent genetic studies[6] have identified various favourable adiposity alleles which are associated with higher BMI, higher subcutaneous to visceral adipose tissue, higher insulin sensitivity, yet lower type 2 diabetes risk.

The minor allele of rs373863828 (p.Arg457Gln), found uniquely in populations from the islands of the Pacific, encoding cAMP-responsive element binding protein 3 (CREB3) factor regulatory (CREBRF) is associated with the largest increase in BMI reported for a common gene variant (approximately 1.4kg/m2 per allele) yet intriguingly, 1.6-fold decrease in the risk of type 2 diabetes[7-11]. CREBRF, expressed widely in a variety of tissues, is a specific negative regulator of CREB3; it can translocate nuclear CREB3 out of the nucleus and promote CREB3 protein degradation, which regulates the CREB3/Luman protein localized at the endoplasmic reticulum CREBRF (CREB3 regulatory factor)[12]. Furthermore, all CREB3 family sub-members play a role in unfolded protein response[12,13]. CREBRF is a potent tumor suppressor of glioblastoma that functions by blocking hypoxia-induced autophagy and is also involved in the regulation of angiogenesis by high-density lipoproteins[14-16]. While the CREB3/Luman protein was identified through its association with herpes simplex virus-related host cell factor 1, indicating that this

protein may play a role in virus emergence from latency[17] , its mechanistic effects on obesity or type 2 diabetes is unclear.

Appropriate animal models are necessary to define the function of the CREBRF in relation to obesity and mechanisms for protection from T2DM. To date, most studies of CREBRF p.Arg457Gln are limited to the description of phenotypes among specific human populations[18-24]. The CREBRF knock-out mice has been used to examine anxiety-like behavior and circulating glucocorticoids in response to various acute stress conditions[25,26]. Orthologous mouse CREBRF p.Arg458Gln variant gene knock-in mice showed increase in length at 8 weeks post birth, but showed no significant difference in body mass or fasting glucose or insulin at 10 weeks[21] Compared with rodents, the anatomy, physiology, size of organ, and life expectancy of pigs are more similar to humans[27,28]. The circadian rhythm (diurnal), eating behavior (discontinuously during the day), fat composition and deposition, gastrointestinal structure, islet structure, beta cell mass, insulin, and endocrine cell type proportion of pigs are similar to humans[29-37]. Pigs may be more suitable animal models for studying the relationship between obesity and type 2 diabetes among different genotypes[38].

Here, we generated a CREBRF missense variant pig model with p.Arg457Gln mutations anchored in exon 7 via the CRISPR/Cas9 system. CREBRF p.Arg457Gln pigs fed with normal chow diet have elevated fat deposition and insulin sensitivity, thereby authentically replicating the phenotypes of human population with p.Arg457Gln mutations. The obesity of pigs with the CREBRF p.Arg457Gln variant was caused by increased number rather than size of adipose tissues. Moreover, the reduced risk of obesity-induced type 2 diabetes was found to be related to the lower reactive oxygen species in the adipose tissue, which would prevent insulin resistance. This study provides a new perspective for the metabolically healthy adiposity resulting from *CREBRF* p.Arg457Gln.

# Results

### Generation of CREBRF p.Arg457Gln pigs and germline transmission of the variant

A CRISPR/Cas9-mediated, HR-dependent integration strategy was used to introduce the corresponding human mutation p.Arg457Gln (c.1370G>A) into porcine endogenous CREBRF locus. First, we compared the protein sequence and coding sequence of human CREBRF with that of pigs and found 99% and 94% homology, respectively. The homologous site of human missense mutation (c.1370G>A) in pig is also c.1370G>A; thus, we designed sgRNA and ssODNs with 89 nt containing c.1370G>A as homology-directed repair (HDR) donor template to introduce the missense mutation (c.1370G>A) into the pig CREBRF gene (Figure 1A). Similar sense mutations were introduced in the ssODNs at the single-guide RNA (sgRNA) target site to avoid retargeting (Fig. 1a).

The Cas9-gRNA plasmid and CREBRF c.1370G>A ssODNA were co-transfected into pig fetal fibroblast cells (PFFs) derived from 35-day-old fetus through electroporation. After selection using G418 for 7–9 days, 370 cell clones were selected and expanded. The sequencing of the PCR products of the objective

DNA fragment confirmed that 14 of 370 cell colonies were modified with the biallelic mutation (CREBRF $^{c.1370G>A/\ p.1370G>A}$). Cell colony nos. 49, 75, 289, 327, and 358 were used as donor cells for somatic cell nuclear transfer (SCNT) (Fig. 1e). A total of 843 cloned embryos were transferred into the oviducts of four recipient surrogates. Three of them were pregnant and gave birth to 12 piglets including 7 females and 5 males (Fig. 1c, 1d and 1e). The genotyping results indicated that all 12 cloned piglets were homozygous for the mutated CREBRF gene (CREBRF$^{c.1370G>A/\ c.1370G>A}$, Fig. 1b). Two CREBRF p.Arg457Gln variant female founders were mated to two wild-type (WT) Bama male pigs and gave birth to 24 first-generation (F1) offspring. PCR genotyping (Fig. 1b) revealed that 17 of the 24 F1 pigs carried the CREBRF variant including 5 female homozygotes, 2 male homozygotes, 7 male heterozygotes, and 3 female heterozygotes (Fig. 1e). These results validate the feasibility of germline transmission of CRISPR/Cas9-based genetic engineering in pigs and indicate that the CREBRF p.Arg457Gln variant might not affect fertility.

## CREBRF p.Arg457Gln variant pigs displayed obesity and lower insulin resistance

In humans, the CREBRF p.Arg457Gln variant is inherited in an autosomal-dominant pattern and is known to strongly associate with body mass index (BMI), including body fat percentage, abdominal circumference, and height[7,8]. Hence, we then characterized the metabolic phenotype of the CREBRF p.Arg457Gln variant pigs. As predicted, the body weight of CREBRF p.Arg457Gln variant pigs significantly increased compared with that of the control (Fig. 2a) (WT, **vs. ** $p<0.05$). Body length and abdominal circumference were elevated in CREBRF p.Arg457Gln pigs (Fig. 2b and 2c) (**vs. ** $p<0.05$, **vs. ** $p<0.05$ ). Computer tomography (CT) scan-based body composition analysis revealed that the majority of the body mass difference between the CREBRF p.Arg457Gln variant and wild-type pigs was attributed to fat deposition when fed on a chow diet (Fig. 2d). The mRNA expression of CREBRF was not negatively affected (Fig. 2e), while protein expression was not changed in subcutaneous fat tissues of homozygous CREBRFc.1370G>A/ c.1370G>A pigs (Fig. 2f). After dissection, white adipose tissue (WAT) appeared thicker in the CREBRF p.Arg457Gln variant pigs (data not show). Histological analysis revealed smaller but more abundant lipid accumulation in the subcutaneous adipose tissue (SAT) of the CREBRF p.Arg457Gln variant pigs than that in the control (Fig. 2g and 2h)".

Similar to humans, CREBRF p.Arg457Gln pigs also displayed lower fasting glucose and insulin levels. Glucose tolerance evaluated by intravenous glucose tolerance test (IGTT) (Fig. 2i) revealed that the blood glucose level increased rapidly in CREBRF p.Arg457Gln variant pigs and wild-type pigs shortly after glucose injection but it returned to the basal level faster in variant pigs than in WT ones. The insulin tolerance test (ITT) showed that the blood glucose level reduced more quickly and maintained low for longer time in variant pigs after insulin injection (Fig. 2j) than that in WT counterpart. These data indicate that CREBRF p.Arg457Gln variant pigs were predisposed to obesity and might have improved insulin sensitivity, consistent to the phenotypic correlation in CREBRF p.Arg457Gln variant in humans.

## CREBRF p.Arg457Gln enhanced preadipocyte differentiation in WAT

The morphology and size of adipocytes were examined in the SAT of 10-week-old CREBRF p.Arg457Gln variant and wild-type pigs to further investigate the obesity phenotype. Histological analysis and hematoxylin-eosin staining (Fig. 2g and 2h) showed that adipocyte size was obviously smaller in the SAT of CREBRF p.Arg457Gln variant pigs accompanied with increased adipocyte number. We also examined the phenotype of adipocytes through in vitro culture. We isolated the precursor adipocytes from subcutaneous adipose tissues and differentiated them into mature adipocytes. The differentiation method was modified from Zheng[39], and the transformation rate was close to 90%. As predicted, the precursor adipocytes from CREBRF p.Arg457Gln variant pigs produced more mature adipocytes in vitro than from the wild-type littermates (Fig. 2k and 2l). This finding suggests that CREBRF p.Arg457Gln promotes the differentiation of precursor adipocytes.

We explored the molecular basis of CREBRF p.Arg457Gln-mediated fat deposition in SAT. A global comparison of the mRNA expression profile of the CREBRF p.Arg457Gln variant and wild-type pigs was performed (Fig. 3). At a threshold of 1.5-fold change, RNA sequencing (RNA-seq) analysis identified 667 significantly up-regulated genes and 1126 significantly down-regulated genes in the CREBRF p.Arg457Gln variant relative to the wild type (Fig. 3a). These differently expressed genes were found to be involved in multiple gene ontology (GO) terms, such as cell proliferation, energy metabolism, ion response, and fat metabolism. Pathway enrichment analysis markedly focused on the PPAR signaling pathway (Fig. 3b) and showed that the mRNA expression levels of several genes related to adipocyte differentiation (*ANGPTL4*, *SORBS1*, *ACDC*, *PLIN2*, *PLIN4*, and *PLIN5*) were significantly up-regulated in the CREBRF p.Arg457Gln variant pigs ($P < 0.01$) (Fig. 3c). We observed that fatty acid synthesis-related genes strongly preferred to present in the down-regulated gene regions ($P < 0.01$), such as *SCD*, *ACAT2*, *FASN*, *ECHS1*, *ELOVL6*, *FADS1*, *FADS2*, and *TECR*. These findings were also confirmed by quantitative PCR (qPCR) test (Fig. 3d).

Overall, CREBRF p.Arg457Gln regulated fat deposition probably by promoting adipocyte differentiation, rather than accelerating the de novo lipogenesis of adipocyte, which result in increased adipocyte number instead of expanding its size.

## CREBRF p.Arg457Gln improved insulin sensitivity through repression of oxidative capacity

CREBRF p.Arg457Gln variant pigs exhibited elevated insulin sensitivity. To further identify changes in the global gene expression in CREBRF p.Arg457Gln variant pigs that might account for the observed improvement of glucose uptake, we performed a Gene Set Enrichment Analysis (GSEA) on genes that were significantly different between CREBRF p.Arg457Gln pigs and wild-type ones (Fig. 3b). Gene sets including tricarboxylic acid cycle (TAC) (Fig. 3e and 3g) and oxidative phosphorylation (OXPHOS) (Fig. 3f and 3h) were found to be strongly enriched in the up-regulated but not in the down regulated pool. The plot of the position of each of the 132 genes in the oxidative phosphorylation set showed that the down-regulated genes (87) of oxidative phosphorylation was almost two times more than the up-regulated ones (43). This finding strongly argues that the enrichment of the oxidative phosphorylation set genes in the up-regulated pool is not simply a consequence of the most abundant oxygen metabolism-related genes

detected by the RNA-seq, which is a phenotype caused by the CREBRF missense mutation. Metabolome analysis revealed the accumulation of the intermediates of glycolysis (Fig. 4a, 4b and 4c), including phosphoenolpyruvate (PEP) in CREBRF p.Arg457Gln variant pigs; meanwhile, glycerone phosphate, N-Acetyl-D-glucosamine 6-phosphate, glutathione disulfide, 1,2-Diacylglycerol-Bile-PC-pool, Phosphodimethylethanolamine, and D-Ribose 5-phosphate were reduced[40,41]. Hence, pigs rendered with the CREBRF p.Arg457Gln variant may probably had lower SAT oxidative capacity .

Excessive production of peroxides in the electron transport chain of mitochondria will increase the number of reactive oxygen species (ROS) and trigger a state of oxidative stress, which could lead to insulin resistance and even type 2 diabetes[42,43]. Repression of oxidative capacity in SAT from CREBRF p.Arg457Gln variant pigs suggests that the reduction of ROS may contribute to the improved insulin sensitivity. To test this idea, we measured the ROS production of SAT from CREBRF p.Arg457Gln and wild-type pigs with a Dihydroethidium (DHE) probe. The CREBRF p.Arg457Gln variant pigs displayed significantly lower ROS than the wild-type pigs (Fig. 5a). We then detected lipid peroxide content in the SAT from CREBRF p.Arg457Gln variant and wild-type pigs. The levels of 4-HNE and MDA evidently decreased in the CREBRF p.Arg457Gln variant pigs (Fig. 5b and 5c). Antioxidant enzyme activity was measured. We observed increased glutathione peroxidase (GPX), superoxide dismutase (SOD), and catalase (CAT) activity (Fig. 5d, 5e, 5f and 5g). Correspondingly, the mRNA expression levels of Gpx1, Sod2, and Prdx5 increased. Thus, the transcriptome and metabolome data indicate that the CREBRF p.Arg457Gln variant reduced the oxidative metabolism in SAT.

# Discussion

In this study, we generated and characterized a pig model with missense CREBRF p.Arg457Gln variant by combining CRISPR/Cas9 editing system with somatic cell nuclear transfer. CREBRF p.Arg457Gln pigs fed with normal chow diet have elevated fat deposition and insulin sensitivity at around 20 weeks old, authentically replicating the increased BMI yet reduced risk of type 2 diabetes phenotypes observed in human populations with p.Arg457Gln mutations.

We obtained 12 homozygous founder pigs with females and males. Seventeen F1 pigs were identified as CREBRF p.Arg457Gln variant carriers with heterogeneous and homozygous mutations. All the CREBRF p.Arg457Gln variant carriers, regardless of heterozygote or homozygote, male or female, displayed obviously increased body weight, abdominal circumference, and body length compared with the wild-type littermates. All these phenotypes were resulted from normal diet chow, similar to the human population with the same genotype[19,21-23]. The model is different from obesity linked to diabetes models, such as over-expressing fat mass and obesity-associated (FTO) mice[44], mice with genetic deletions of melanocortin 4 receptor(MC4R)[45] leptin-deficient mice[46] and zebrafish obesity models[47], in which the obesity phenotype was primarily caused by increased appetite and food intake and decreased physical activity[48]. The CREBRF p.Arg457Gln pigs could store more fat without overeating. Moreover, mutations in

the FTO gene often lead to the development of abnormalities[49-51], which was not seen among CREBRF p.Arg457Gln pigs[42].

According to the location of deposition, fat can be divided into visceral fat and subcutaneous fat. In the CREBRF p.Arg457Gln variant pigs, body weight gain could be ascribed to increased fat deposition mainly in subcutaneous fat given that we did not observed distinct fat accumulation in the visceral organ (data not shown). The CT results also confirmed limited visceral but mainly increaced subcutaneous fat deposition in CREBRF p.Arg457Gln variant pigs. The metabolically unhealthy obesity phenotype is associated with enlarged adipocytes with reduced buffering capacity for lipid storage, thereby exposing organs, such as liver, skeletal muscle, pancreas, the heart, and kidneys, to an excessive influx of lipids, leading to ectopic fat deposition and insulin resistance[52,53]. Ectopic lipid deposition is deleterious[54-56], while deep abdominal subcutaneous adipose tissues seem to be “metabolically healthy,” and were proven to have higher expression of pro-inflammatory, lipogenic, and lipolytic genes and contain higher proportions of saturated fatty acids and small adipocytes[57,58]. Increased capacity for subcutaneous fat deposition in the CREBRF p.Arg457Gln variant pigs suggests that this obesity may confer lower risk for type 2 diabetes.

The insulin resistance of adipocytes is recognized as one of the hallmarks of type 2 diabetes pathogenesis[59]. IGTT and ITT data indicated that CREBRF p.Arg457Gln variant pigs have improved insulin sensitivity, consistent with the phenotypic correlation in humans with the CREBRF p.Arg457Gln variant. Previous reports showed that excessive free fatty acid (FFA) in circulation is related to obesity, insulin resistance, and type 2 diabetes. Adipocytes can efficiently sequester excessive glucose and fatty acids from the circulation and store them in intracellular lipid droplets[60]. When an individual becomes obese, adipocytes expand and become hypertrophic with intracellular lipid accumulation; they eventually rupture and fatty acids flow out[61-64], thereby inhibiting insulin-stimulated glucose transport or phosphorylation, and glycogen synthase activity[65,66]. The adipocytes of SAT in CREBRF p.Arg457Gln variant pigs had smaller size but increased number, suggesting that the CREBRF p.Arg457Gln variant increases the storage capacity of adipose tissue by promoting the differentiation of adipocyte progenitor cells into more adipocytes (hyperplasia) instead of expanding their size (hypertrophy). The RNA-seq data also confirmed that adipogenic differentiation associated peroxisome proliferator-activated receptor (PPAR) signaling pathway was significantly enriched and fatty acid transportation-related genes were obviously down-regulated in the CREBRF p.Arg457Gln variant pigs. We also validated adipocyte hyperplasia through examination of the differentiation capacity of preadipocyte cells in vitro. More new adipocytes were generated from the same number of CREBRF p.Arg457Gln preadipocytes than the wild-type ones. Therefore, pigs with the CREBRF p.Arg457Gln variant contain numerous and relatively smaller adipocytes, which improve their energy storage capability before enlarging and risking toxic ectopic lipid accumulation related rupture of hypertrophic adipocytes and subsequent increased plasma FFA level and insulin resistance. Palmitoleic acid, which has beneficial effects on glucose homeostasis in dietary obesity and a potential target for development of diabetes drugs[67], was greatly enhanced in the CREBRF p.Arg457Gln variant

pigs. This finding also suggests the important role of the CREBRF p.Arg457Gln variant in type 2 diabetes protection.

Increasing lines of evidence in experimental and clinical studies suggest that obesity causes redox imbalance in fat tissues and produces excessive ROS and harmful free radicals, which result in oxidative stress. Oxidative stress is thought to contribute to diabetes progression by inducing insulin resistance[68-72]. In the present study, several mechanisms by which the CREBRF p.Arg457Gln variant could attenuate adipocytes oxidative stress were identified, including down-regulating OXPHOS and reducing ROS production. The particular reaction of ROS with lipids is generally known as “lipid peroxidation.” 4-Hydroxy-nonenal (HNE) and malondialdehyde (MDA) are the most frequently measured biomarkers of lipid peroxidation[73]. The levels of 4-HNE and MDA in the SAT of CREBRF p.Arg457Gln variant pigs decreased, representing the decline in lipid peroxidation. Accordingly, preoxidative metabolites, such as glycerone phosphate, N-Acetyl-D-glucosamine 6-phosphate, glutathione disulfide, 1,2-Diacylglycerol-Bile-PC-pool, Phosphodimethylethanolamine, and D-Ribose 5-phosphate[40,41], were reduced. Oxidative stress occurs when excessive formation of ROS overwhelms the antioxidant defense system, including glutathione peroxidase (GPX), superoxide dismutase (SOD), and catalase (CAT)[74,75]. The mRNA expression levels of Gpx1, Sod2, and Prdx5 increased, indicating that the activities of antioxidant enzymes were enhanced, which would detoxify ROS, prevent the harmful effects of active oxidizing reaction, and maintain redox homeostasis. Therefore, there was lower risk of obesity- induced type 2 diabetes in pigs with the CREBRF p.Arg457Gln variant.

In summary, these pig studies demonstrate that p.Arg457Gln variant in CREBRF promotes the differentiation of precursor adipocytes into more mature adipocytes for storing more energy by increasing their number (hyperplasia) rather than their size (hypertrophy). Secondly, the p.Arg457Gln variant in CREBRF reduces oxidative capacity and increases the antioxidative ability of SAT, thereby scavenging excess ROS. Both effects of the CREBRF p.Arg457Gln variant reduce insulin resistance and reduce the risk of type 2 diabetes (Fig. 6).

# Materials And Methods

### Ethics Statement and Animal Housing

All experiments involving animals were conducted according to the guidelines for the care and use of laboratory animals established by the Guangdong Association for Laboratory Animal Science and approved by the Animal Ethics Committee of the Guangzhou Institutes of Biomedicine and Health, Chinese Academy of Sciences. Pigs were raised at the Jiangmen Farm Animal Research Center. Feed was given twice daily without limit.

### Plasmids

Given that Arg457 in the pig CREBRF protein was identified as homologous to human Arg457 that is mutated in Samoans, we planned to introduce a point mutation homologous to human p.Arg457Gln on exon 7 of the pig CREBRF gene by using CRISPR/Cas9-based genome editing. The sequences are listed in Supplementary Table 1. The pig endogenous CREBRF fragment was cloned into the U6-gRNA vector along with the annealed sgRNA oligos, which were designed using the tool available at the website http://crispr.mit.edu, to construct a targeting vector. Additionally, a donor oligonucleotide was used to mutate CGA encoding Arg457 to CAA (encoding Gln) by homology-directed repair. The CRISPR/Cas9 construct was obtained as previously described.

### Cell Culture and Transfection

Primary pig PFFs were isolated as previously reported[76]. Targeting vector CRISPR/Cas9 construct were co-injected with the donor oligonucleotide into cultured PFF cells by electrotransfection. Forty-eight hours after transfection, cells were harvested using 0.25% trypsin/EDTA (Gibco), and the cell density was calculated using a handheld automated cell counter (Millipore). Single cells were plated in each well of 96-well plates by limiting dilution and cultured for ~10 d in the cell culture medium supplemented with 2.5 ng/mL basic fibroblast growth factor (Sigma). The medium was replaced every 3 days. Confluent cell colonies were propagated and genotyped by PCR and sequencing.

### Nuclear Transfer and Embryo Transfer

Pig ovaries were collected from a local slaughterhouse and transported to the laboratory within 1 h in 0.9% saline maintained at 37 °C. The in vitro maturation of oocytes, enucleation, microinjection, and the fusion of reconstructed oocytes were performed in our laboratory according to previously described methods. The reconstructed embryos were cultured in porcine zygote medium in 5% $CO_2$ at 39 °C for 14-16 h until embryo transfer. Embryos in good condition were surgically transferred into the oviduct of a surrogate the day after observed estrus. Gestation was detected by ultrasound at day 28 after embryo transfer. All of the cloned piglets were delivered by natural birth.

### RNA Preparation and qPCR Analysis

Total RNA was isolated from pig SAT with TRIzol (Invitrogen). First-strand cDNA synthesis was performed using a FastQuant RT Kit (Tiangen Biotech). Quantitative real-time PCR reactions were performed using SYBR Premix Ex Taq (Tli RNaseH Plus; Takara) on an Agilent Mx3005p (Agilent Technologies) with reaction volume of 20 μL. The primer sequences are listed in Supplementary Table 2. Relative gene expression was calculated using comparative cycle threshold ($2^{-\Delta\Delta Ct}$) method. Statistical analysis was performed with GraphPad Prism 8.0.

### Western Blot Analysis

SAT were dissected, frozen immediately in liquid nitrogen, and stored at -80 °C until use. Total proteins from tissue or cultured adipocyte were extracted using the Minute Total Protein Extraction Kit (Invent

Biotechnologies, Inc.). The proteins were subjected to Western blot analysis with the following antibodies: anti-CREBRF (PA5-68552, 1:1000; Invitrogen, Inc.), and anti-actin (AF7018,1:2000, Affinity). The blots were developed using HRP-conjugated secondary antibodies and an ECL Plus system. All signals were visualized and analyzed with a Tanon 5200 (Tanon Science & Technology Co. Ltd.)

### Computed tomography (CT)

Ten-week-old female Bama pigs of the CREBRF R457R variant and wild type were used for the experiments. All pigs were clinically healthy based on physical examination. CT was conducted using a helical CT scanner with a single-detector CT (GE Medical System, USA) beginning at the upper edge of the liver and continuing caudally to the L4 level. The pigs were placed under general anesthesia for the procedure. Image acquisition parameters included a matrix of 512 × 512, a large-scan field of view, a 1.25 mm slice thickness, 120 kVp, 60 mA, and a pitch of 1.3. CT scans were conducted to determine the distribution of abdominal fat identified based on the number measured in Hounsfield Units (HU). CT number ranges of visceral and subcutaneous abdominal adipose tissue were obtained by manually setting the region of interests (ROIs) corresponding to each of the images obtained at the L3, L4 levels by three radiologists. In this procedure, we defined the attenuation range of fat tissue from -190 HU to -32 HU. By adjusting the fat ranges, we easily obtained the areas of total abdominal fat by using the built-in software for the helical CT scanner. We then compared the overall abdominal fat mass with the fat areas calculated at the L3 and L4 levels by defining them as landmarks to measure the total abdominal fat distribution.

### Histological Analysis

Adipose tissues were fixed in 4% paraformaldehyde/1× PBS overnight at 4 °C and dehydrated through sequential ethanol washes. The tissue was embedded in paraffin before sectioning and then stained with hematoxylin and eosin. The stained sections were visualized and photographed under bright-field microscopy.

### Glucose Tolerance Test

For intravenous glucose tolerance tests, pigs were fasted for 16 h and challenged with intravenous injection of 50% glucose (1.2 mL/kg body weight). For insulin tolerance tests, pigs were fasted for 12 h and then given an intraperitoneal injection of insulin (0.75 U/kg body weight). Blood glucose levels were measured by using a glucose monitor (Accu-Chek. Performa, Roche, Germany) in blood drawn from the auricular region at 0, 5, 10, 15, 30, 45, 60, 90, and 120 min.

### Transcriptome Profiling

Total RNA was extracted using Trizol reagent kit (Invitrogen, Carlsbad, CA, USA) according to the manufacturer’s protocol. RNA quality was assessed on an Agilent 2100 Bioanalyzer (Agilent Technologies, Palo Alto, CA, USA) and checked using RNase-free agarose gel electrophoresis. After total RNA was extracted, eukaryotic mRNA was enriched by Oligo(dT) beads. The enriched mRNA was

fragmented into short fragments by using fragmentation buffer and reverse transcribed into cDNA with random primers. Second-strand cDNA was synthesized by DNA polymerase I, RNase H, dNTP, and buffer. The cDNA fragments were purified with QiaQuick PCR extraction kit (Qiagen, Venlo, The Netherlands), end repaired, poly(A) added, and ligated to Illumina sequencing adapters. The ligation products were size selected by agarose gel electrophoresis, PCR amplified, and sequenced using Illumina HiSeq2500 by Gene Denovo Biotechnology Co. (Guangzhou, China). Raw reads were mapped against the reference genome by using HISAT2. 2.4 with “-rna-strandness RF”. The mapped reads were converted to FPKM (fragments per kilobase of exon per million fragments mapped) by running StringTie software to determine gene expression. RNA differential expression was analyzed by DESeq2 software between two different groups (and by edgeR between two samples). The genes/transcripts with the parameter of false discovery rate (FDR) below 0.05 and absolute fold change≥2 were considered differentially expressed genes/transcripts. Gene set enrichment analysis was performed using software GSEA and MSigDB to identify whether a set of genes in specific GO terms/pathways/DO terms shows significant differences in the two groups. Briefly, we input gene expression matrix and rank genes by SinaltoNoise normalization method. Enrichment scores and p value were calculated in default parameters.

## Metabolome analysis

About 50 mg of the sample was weighed to an EP tube. After the addition of 1000 μL of extract solvent (acetonitrile-methanol-water, 2:2:1, containing internal standard), the samples were vortexed for 30 s, homogenized at 45 Hz for 4 min, and sonicated for 5 min in ice-water bath. The homogenization and sonication were repeated three times, followed by incubation at -20 °C for 1 h and centrifugation at 12000 rpm and 4 °C for 15 min. The resulting supernatants were transferred to LC-MS vials and stored at -80 °C until the UHPLC-QE Orbitrap/MS analysis. The quality control (QC) sample was prepared by mixing an equal aliquot of the supernatants. LC-MS/MS analyses were performed using an UHPLC system (1290, Agilent Technologies) with a UPLC HSS T3 column (2.1 mm × 100 mm, 1.8 μm) coupled to Q Exactive (Orbitrap MS, Thermo). The mobile phase A was 0.1% formic acid in water for positive, and 5 mmol/L ammonium acetate in water for negative, and the mobile phase B was acetonitrile. The QE mass spectrometer was used to acquire MS/MS spectra on an information-dependent basis (IDA) during the LC/MS experiment. MS raw data files were converted into the mzML format by using ProteoWizard and processed by R package XCMS (version 3.2), including retention time alignment, peak detection, and peak matching. OSI-SMMS (version 1.0, Dalian Chem Data Solution Information Technology Co. Ltd.) was used for peak annotation after data processing with the in-house MS/MS database. For preliminary visualization of differences between different groups of samples, the unsupervised dimensionality reduction method principal component analysis (PCA) was applied using R package models (http://www.r-project.org/). PLS-DA, a supervised dimensionality reduction method in which class memberships are coded in matrix form into Y to better distinguish the metabolomics profile of two groups by screening variables correlated to class memberships, was applied to compare the groups by using R package models (http://www.r-project.org/). A variable importance in projection (VIP) score of (O)PLS model was applied to rank the metabolites that best distinguished between two groups. The threshold of VIP was set to 1. In addition, T-test was used as a univariate analysis for screening

differential metabolites. Those with a P value of T test<0.05 and VIP≥1 were considered differential metabolites between two groups.

### Porcine Primary Preadipocyte Isolation and in Vitro Differentiation

Adipose tissues were harvested from 2-week-old piglets, minced, and digested with 2 mg/mL collagenase type I (Sigma) in DMEM/F12 containing 1% fatty acidfree BSA (Sigma) for 60 min at 37 °C. Stromal vascular fraction cells were collected with a cell strainer (70 μm diameter), plated, and grown in DMEM/F12 (Gibco) supplemented with 10% FBS (Sigma) and 1% penicillin–streptomycin. For white adipocyte differentiation, cells were grown to confluence and treated with human WAT induction medium [DMEM/H medium containing 0.25 mM isobutylmethylxanthine, 0.1 μM dexamethasone, 66 nM human insulin (Sigma), 17 μM pantothenate, 33 μM biotin, 20 mM Hepes (pH 7.4), and 0.5% FBS] for 5 days. At day 5, half of the induction medium was removed and the same volume of human WAT mature medium [DMEM/H medium containing 10μM rosiglitazone, 0.1 μM dexamethasone, 66 nM human insulin, 17 μM pantothenate, 33 μM biotin, 20 mM Hepes (pH 7.4), and 10% FBS] was added. One day later, the cells were cultured in pure human WAT maturation medium for 2 days and then change the medium every two days. On day 15, cells are fully differentiated and mature adipocytes ready for subsequent experiments.

### ROS Assay

ROS was detected using DHE staining. DHE is a cell-permeable fluorogenic probe that reacts with ROS to form ethidium and emits red fluorescence. Adipose tissues were weighed and homogenized, and then homogenate supernatant was taken, mixed with DHE probe, and incubated in the dark for 30 min at 37 ℃. Fluorescence intensity was detected at the excitation wavelength of 488–535 nm and emission wavelength of 610 nm by using an inverted fluorescence microscope (DP72/CKX41, Olympus). Finally, the reactive oxygen species level of tissues was expressed by fluorescence intensity/mg protein.

### 4-HNE and MDA Analysis

4-HNE and MDA was measured by enzyme-linked immunosorbent assay and TBA fluorescence method, respectively. First, adipose tissues were weighed and homogenized, then 4-HNE was detected according to the manufacturer's instruction. First, set blank hole, standard hole, sample hole. Add sample 50 μL accurately to the Elisa-coated plate, add sample dilution 40 μL to the test sample well, then add sample 10 μL to the test well. Add the sample to the bottom of the enzyme plate well and mix gently. Then, after sealing the plate with sealing plate membrane, incubate at 37℃ for 30 minutes. Uncover sealing plate membrane, discard liquid, dry by swing, add washing solution to each well, rest for 30 seconds and then drain, repeat 5 times. Add HRP-conjugate reagent 50 μL to each well, except blank well. Incubate at 37℃ for 30 minutes and wash. Afterwards, add chromogenic agent A 50 μL and chromogenic agent B 50 μL to each well, mix gently. Add stop solution 50 μL to each well at 37℃ for 10 min away from light, stop the reaction. Finally, the absorbance of each hole was measured in sequence at 450 nm wavelength with blank air conditioning zero. MDA was detected by mixed TBA dye, and fluorescence intensity was detected at the absorbance wavelength of 532 nm by using a microplate reader.

### GPX, SOD, and CAT Assay

GPX, SOD, and CAT assays were conducted using exclusive kits according to the manufacturer's instructions (H545-1, A001-3-1 andA007-1-1; Nanjing Jiancheng Bioengineering Institute). For detail operation steps, please refer to the commercial manual.

### Oil Red Staining of Mature Adipocytes

Adipocytes in one well of the six-well plate were used as an example. The cells were gently washed twice with PBS and fixed with 500 μL of 4% paraformaldehyde for 30 min. Oil red working liquid was prepared: Distilled water = 3:2, mix and filter through a 70 μM filter. After the cells were fixed, they were washed with 500 μL 60% isopropanol, excess water was removed, and the cells were turned upside down until they were completely dried. The sample was added with 300 μL of oil red working solution and stained for 10 min without shaking. The oil red working fluid was absorbed, and the cells were gently washed with $DDH_2O$ for 4 times. After washing, the supernatant was absorbed and discarded. The sample was placed under a microscope, and photos were taken. For further absorbance test, the excess $DDH_2O$ should be completely absorbed and dried. The sample was added with 750 μL of 100% isopropyl alcohol and incubated for at least 10 min. Gentle blowing was conducted to ensure that all the oil red staining solution was dissolved in isopropyl alcohol. The dye solution was transferred to a 1.5mL centrifuge tube. A new 1.5 mL centrifuge tube filled with 100% isopropyl alcohol of the same volume as the control was prepared. OD value was obtained at the wavelength of 500 nm and read in 0.5 seconds.

### Statistical Analysis

The statistical data reported include results from at least three biological replicates. All results are expressed as mean ± SEM. For normal distribution data, differences between two groups were assessed by unpaired Student’s t tests.

# Declarations


### Acknowledgements

This work is supported by National Key Research and Development Program of China Stem Cell and Translational Research (2017YFA0105103), the Strategic Priority Research Program of the Chinese Academy of Sciences (XDA16030503), Biological Resources Progaramme, Chinese Academy of Sciences (KFJ-BRP-017-57), Science and Technology Planning Project of Guangdong Province (2017A050501059, 2020B1212060052, 2021B1212040016, 2020A1515110213 and 2020B1212060052), the Key Research & Development Program of Bioland Laboratory (Guangzhou Regenerative Medicine and Health Guangdong Laboratory) (2018GZR110104004 and 2018 GZR110105019), Science and Technology Program of Guangzhou, China (202007030003), 2020 Research Program of Sanya Yazhou Bay Science and Technology City (202002011), Research Unit of Generation of Large Animal Disease Models, Chinese Academy of Medical Sciences (2019-I2M-5-025).

### Author contributions

Y.L., H.W. and Y.L. performed experiments. Q.Y. provided valuable suggestions about experimental design. Z.O., Y. Z., Q. Z., C. L., and Z.L. helped with SCNT. Z. Z. helped with the PFF cell clones screening. H. L., S. Z., J .W., C . L., Y. S., T. L. and Y. L., helped with preadipocyte differentiation. Y. Y. helped with the RNA-seq data analysis. Q. Z., Z. D., and T. N. helped with the metabolome data analysis. N.F. and L. L. were responsible for the study concept and design. Y.L. and H. W. wrote the manuscript. D. W., N.F. and L. L. supervised the study. All authors approved the final version of the manuscript.

### Competing interests

The authors declare no competing interests.

# References


1. Muhammad, L. J., Algehyne, E. A. & Usman, S.S. Predictive Supervised Machine Learning Models for Diabetes Mellitus. *SN Comput Sci.* **1**, 240 (2020).

2. Koh-Banerjee, P. et al. Changes in body weight and body fat distribution as risk factors for clinical diabetes in US men. *Am. J. Epidemiol.* **159**, 1150-1159 (2004).

3. Shai, I. et al. Ethnicity, obesity, and risk of type 2 diabetes in women: a 20-year follow-up study. *Diabetes Care* **29**, 1585-1590 (2006).

4. Wang Y. et al. Comparison of abdominal adiposity and overall obesity in predicting risk of type 2 diabetes among men. *Am. J. Clin. Nutr.* **81**, 555-563 (2005).

5. Toplak, H. et al. Obesity and type 2 diabetes. *Wien. Klin. Wochenschr.* **128**, S196-200 (2016).

6. Yaghootkar L. et al. Genetic Evidence for a Link Between Favorable Adiposity and Lower Risk of Type 2 Diabetes, Hypertension, and Heart Disease. *Diabetes* **65**, 2448-60 (2016).

7. Minster, R. L. et al. A thrifty variant in CREBRF strongly influences body mass index in Samoans. *Nat. Genet.* **48**, 1049-1054 (2016) .

8. Loos, R. J. F., CREBRF variant increases obesity risk and protects against diabetes in Samoans. *Nat. Gene*t. **48**, 976-978 (2016).

9. Krishnan, M. et al. Discordant association of the CREBRF rs373863828 A allele with increased BMI and protection from type 2 diabetes in Maori and Pacific (Polynesian) people living in Aotearoa/New Zealand. *Diabetologia* **61**, 1603-1613 (2018).

10. Hanson, R. L. et al. Association of CREBRF variants with obesity and diabetes in Pacific Islanders from Guam and Saipan. *Diabetologia* **62**, 1647-1652 (2019).

11. Krishnan, M. et al. The Pacific-specific CREBRF rs373863828 allele protects against gestational diabetes mellitus in Maori and Pacific women with obesity. *Diabetologia* **63**, 2169-2176 (2020).

12. Audas, T. E., Li, Y., Liang, G. & Lu, R. A novel protein, Luman/CREB3 recruitment factor, inhibits Luman activation of the unfolded protein response. *Mol. Cell Biol.* **28**, 3952-3966 (2008).

13. Chan, C. P., Kok, K. H. & Jin, D. Y. CREB3 subfamily transcription factors are not created equal: Recent insights from global analyses and animal models. *Cell Biosci.* **1**, 6 (2011).

14. Xue, H. et al. CREBRF is a potent tumor suppressor of glioblastoma by blocking hypoxia-induced autophagy via the CREB3/ATG5 pathway. *Int. J. Oncol.* **49**, 519-528 (2016).

15. Xue, H. et al. A novel tumor-promoting mechanism of IL6 and the therapeutic efficacy of tocilizumab: Hypoxia-induced IL6 is a potent autophagy initiator in glioblastoma via the p-STAT3-MIR155-3p-CREBRF pathway. *Autophagy* **12**, 1129-1152 (2016) .

16. Wong, N. K. P. et al. Exploring the Roles of CREBRF and TRIM2 in the Regulation of Angiogenesis by High-Density Lipoproteins. *Int. J. Mol. Sci.* **19**, 1903 (2018).

17. Audas, T. E. et al. Characterization of nuclear foci-targeting of Luman/CREB3 recruitment factor (LRF/CREBRF) and its potential role in inhibition of herpes simplex virus-1 replication. *Eur. J. Cell Biol.* **95**, 611-622 (2016).

18. Naka, I. et al. A missense variant, rs373863828-A (p.Arg457Gln), of CREBRF and body mass index in Oceanic populations. *J. Hum. Genet.* **62**, 847-849 (2017).

19. Ohashi, J. et al. Association study of CREBRF missense variant (rs373863828:G > A; p.Arg457Gln) with levels of serum lipid profile in the Pacific populations. *Ann. Hum. Biol.* **45**, 215-219 (2018).

20. Berry,S. D. et al. Widespread prevalence of a CREBRF variant amongst Maori and Pacific children is associated with weight and height in early childhood. *Int. J. Obes (Lond).* **42**, 603-607 (2018).

21. Metcalfe, L.K., Krishnan, M., Turner,N., Yaghootkar, H., Merry, T. L., Dewes, O., et al. The Maori and Pacific specific CREBRF variant and adult height. *Int J Obes (Lond).* **44**, 748-752 (2020).

22. Carlson, J. C. et al. A missense variant in CREBRF is associated with taller stature in Samoans. *Am. J. Hum. Biol.* **32**, e23414 (2020).

23. Hawley, N. L. et al. Exploring the Paradoxical Relationship of a Creb 3 Regulatory Factor Missense Variant With Body Mass Index and Diabetes Among Samoans: Protocol for the Soifua Manuia (Good Health) Observational Cohort Study. *JMIR Res. Protoc.* **9**, e17329 (2020).

24. Arslanian, K. J. et al. A missense variant in CREBRF, rs373863828, is associated with fat-free mass, not fat mass in Samoan infants. *Int. J. Obes (Lond).* **45**, 45-55 (2021).

25. Martyn, A. C. et al. Luman/CREB3 recruitment factor regulates glucocorticoid receptor activity and is essential for prolactin-mediated maternal instinct. *Mol. Cell Biol*. **32**, 5140-5150 (2012).

26. Frahm, K. A. et al. Loss of CREBRF Reduces Anxiety-like Behaviors and Circulating Glucocorticoids in Male and Female Mice. *Endocrinology* **161**, bqaa163 (2020).

27. Aigner, B. et al. Transgenic pigs as models for translational biomedical research. *J. Mol. Med*. **88**, 653-664 (2010).

28. Zettler, S. et al. A decade of experience with genetically tailored pig models for diabetes and metabolic research. *Anim. Reprod*. **17**, e20200064 (2020).

29. Renner, S. et al. Comparative aspects of rodent and nonrodent animal models for mechanistic and translational diabetes research. *Theriogenology* **86**, 406-421 (2016).

30. Spurlock, M. E. & Gabler, N. K. The Development of Porcine Models of Obesity and the Metabolic Syndrome. *J. Nutr*. **138**, 397–402 (2008).

31. Renner, S. et al. Porcine models for studying complications and organ crosstalk in diabetes mellitus. *Cell Tissue Res*. **380**, 341-378 (2020).

32. Hoang, D. T. et al. A conserved rule for pancreatic islet organization. *PloS One*. **9**, e110384 (2014) .

33. Dufrane, D. et al. Impact of porcine islet size on cellular structure and engraftment after transplantation: adult versus young pigs. *Pancreas*. **30**, 138–147 (2005).

34. Kim, S. et al. Molecular and genetic regulation of pig pancreatic islet cell development. *Development* **147**, dev186213 (2020).

35. Bakhti, M., Böttcher, A. & Lickert, H., Modelling the endocrine pancreas in health and disease. *Nat. Rev. Endocrinol.* **15**, 155–171 (2019).

36. Kang, J. D. et al. Apancreatic pigs cloned using Pdx1-disrupted fibroblasts created via TALEN-mediated mutagenesis. *Oncotarget*. **8**, 115480–115489 (2017).

37. Sheets, T. P. et al. Targeted mutation of NGN3 gene disrupts pancreatic endocrine cell development in pigs. *Sci. Rep*. **8**, 3582 (2018).

38. Zhang, L. et al. Development and genome sequencing of a laboratory-inbred miniature pig facilitates study of human diabetic disease. *iScience* **19**, 162–176 (2019).

39. Zheng, Q. et al. Reconstitution of UCP1 using CRISPR/Cas9 in the white adipose tissue of pigs decreases fat deposition and improves thermogenic capacity. *Proc. Natl. Acad. Sci. U. S. A*. **114**, E9474-E9482 (2017).

40. Thornalley, P. J., Langborg, A., Minhas, H. S. Formation of glyoxal, methylglyoxal and 3-deoxyglucosone in the glycation of proteins by glucose. Biochem. J. **344**,109-116(1999).

41. Ighodaro, O. M. Molecular pathways associated with oxidative stress in diabetes mellitus. Biomed. Pharmacother. **108**, 656-662 (2018).

42. Murdolo, G. et al. Oxidative stress and lipid peroxidation by-products at the crossroad between adipose organ dysregulation and obesity-linked insulin resistance. *Biochimie*. **95**, 585-594 (2013).

43. Jankovic, A. et al. Redox implications in adipose tissue (dys)function–A new look at old acquaintances. *Redox Biol*. **6**, 19-32 (2015).

44. Church, C. et al. Overexpression of Fto leads to increased food intake and results in obesity. *Nat. Genet*. **42**, 1086-1092 (2010).

45. Leeners, B., Geary, N., Tobler, P. N., & Asarian, L. Ovarian hormones and obesity. *Hum. Reprod Update* **23**, 300-321 (2017).

46. Tsai, Y. T. et al. Antrodia cinnamomea Confers Obesity Resistance and Restores Intestinal Barrier Integrity in Leptin-deficient Obese Mice. *Nutrients* **12**, 726 (2020).

47. Oka, T. et al. Diet-induced obesity in zebrafish shares common pathophysiological pathways with mammalian obesity. *BMC Physiol*. **10**, 21 (2010).

48. Andreasen, C. H. et al. Low physical activity accentuates the effect of the FTO rs9939609 polymorphism on body fat accumulation. *Diabetes* **57**, 95-101 (2008).

49. Thron, C. et al. FTO Is Associated with Aortic Valve Stenosis in a Gender Specific Manner of Heterozygote Advantage: A Population-Based Case-Control Study. *PLoS One*. **10**, e0139419 (2015).

50. Chen, J. & Du, B. Novel positioning from obesity to cancer: FTO, an m 6 A RNA demethylase, regulates tumour progression. *J. Cancer Res. Clin. Oncol*. **145**, 19-29 (2019).

51. Annapoorna, P. K. et al. FTO: An Emerging Molecular Player in Neuropsychiatric Diseases. *Neuroscience* **418**, 15-24 (2019).

52. Goossens, G. H. The role of adipose tissue dysfunction in the pathogenesis of obesity-related insulin resistance. *Physiol. Behav*. **94**, 206-18 (2008).

53. Stinkens, R., Goossens, G. H., Jocken, J. W. E. & Blaak, E. E. Targeting fatty acid metabolism to improve glucose metabolism. *Obes. Rev*. **16**, 715–757 (2015).

54. Chaurasia, B. & Summers, S. A. Ceramides - Lipotoxic Inducers of Metabolic Disorders. *Trends Endocrinol. Metab*. **26**, 538-550 (2015).

55. Perry, R. J., Samuel, V. T., Petersen, K. F. & Shulman, G. I. The role of hepatic lipids in hepatic insulin resistance and type 2 diabetes. *Nature* **510**, 84-91 (2014).

56. Unger, R. H. Longevity, lipotoxicity and leptin: the adipocyte defense against feasting and famine. *Biochimie*. **87**, 57-64 (2005).

57. Cancello, R. et al. Molecular and morphologic characterization of superficial- and deep-subcutaneous adipose tissue subdivisions in human obesity. *Obesity (Silver Spring)* **21**, 2562-2570 (2013).

58. Marinou, K. et al. Structural and functional properties of deep abdominal subcutaneous adipose tissue explain its association with insulin resistance and cardiovascular risk in men. *Diabetes Care* **3**, 821-829 (2014) .

59. Xue, P. et al. Prolonged inorganic arsenite exposure suppresses insulin-stimulated AKT S473 phosphorylation and glucose uptake in 3T3-L1 adipocytes: involvement of the adaptive antioxidant response. *Biochem. Biophys. Res. Commun*. **407**, 360-365 (2011).

60. Aouadi, M. et al. Lipid storage by adipose tissue macrophages regulates systemic glucose tolerance. *Am. J. Physiol. Endocrinol. Metab*. **307**, E374-383 (2014).

61. Sun, K. , Kusminski, C. M. & Scherer, P. E. Adipose tissue remodeling and obesity. *J. Clin. Invest*.**121**, 2094-2101 (2011).

62. Lefterova, M. I. & Lazar, M. A., New developments in adipogenesis. *Trends Endocrinol. Metab*. **20**, 107-114 (2009).

63. Rosen, E. D. & MacDougald, O. A. Adipocyte differentiation from the inside out, *Nat. Rev. Mol. Cell Biol*. **7**, 885-896 (2006).

64. Tang, Q. Q. & Lane, M.D., Adipogenesis: from stem cell to adipocyte. *Annu. Rev. Biochem*. **81**, 715-736 (2012).

65. Boden, G. Free fatty acids (FFA), a link between obesity and insulin resistance. *Front Biosci*. **3**, d169-75 (1998) .

66. Boden, G. Free fatty acids-the link between obesity and insulin resistance. *Endocr. Pract*. **7**, 44-51(2001).

67. Rossmeisl, M. et al. Increased plasma levels of palmitoleic acid may contribute to beneficial effects of Krill oil on glucose homeostasis in dietary obese mice. *Biochim. Biophys. Acta. Mol. Cell Biol. Lipids* **1865**, 158732 (2020).

68. Maritim, A. C., Sanders, R. A. & Watkins, J. B. Diabetes, oxidative stress, and antioxidants: a review. *J. Biochem. Mol. Toxicol.* **17**, 24-38 (2003).

69. Yang, H., Jin ,X., Lam, C. W. K. & Yan, S. K. Oxidative stress and diabetes mellitus. *Clin. Chem. Lab. Med*. **49**, 1773-1782 (2011).

70. Newsholme, P. et al. Molecular mechanisms of ROS production and oxidative stress in diabetes. *Biochem. J*. **473**, 4527-4550 (2016).

71. Fernández-Sánchez, A. et al. Inflammation, oxidative stress, and obesity. *Int. J. Mol. Sci*. **12**, 3117-3132 (2011).

72. Furukawa, S. et al. Increased oxidative stress in obesity and its impact on metabolic syndrome. *J. Clin. Invest*. **114**, 1752-1761 (2004).

73. Tsikas, D. Assessment of lipid peroxidation by measuring malondialdehyde (MDA) and relatives in biological samples: Analytical and biological challenges. *Anal. Biochem*. **524**, 13-30 (2017).

74. Su L. J. et al. Reactive Oxygen Species-Induced Lipid Peroxidation in Apoptosis, Autophagy, and Ferroptosis. *Oxid. Med. Cell Longev*. **2019**, 5080843 (2019).

75. Liu, J. et al. Peroxisomal regulation of redox homeostasis and adipocyte metabolism. *Redox Biol*. **24**, 101167 (2019).

76. Lai, L. & Prather, R.S. Production of cloned pigs by using somatic cells as donors. *Cloning Stem Cells* **5**, 233-241 (2003).

# Figures

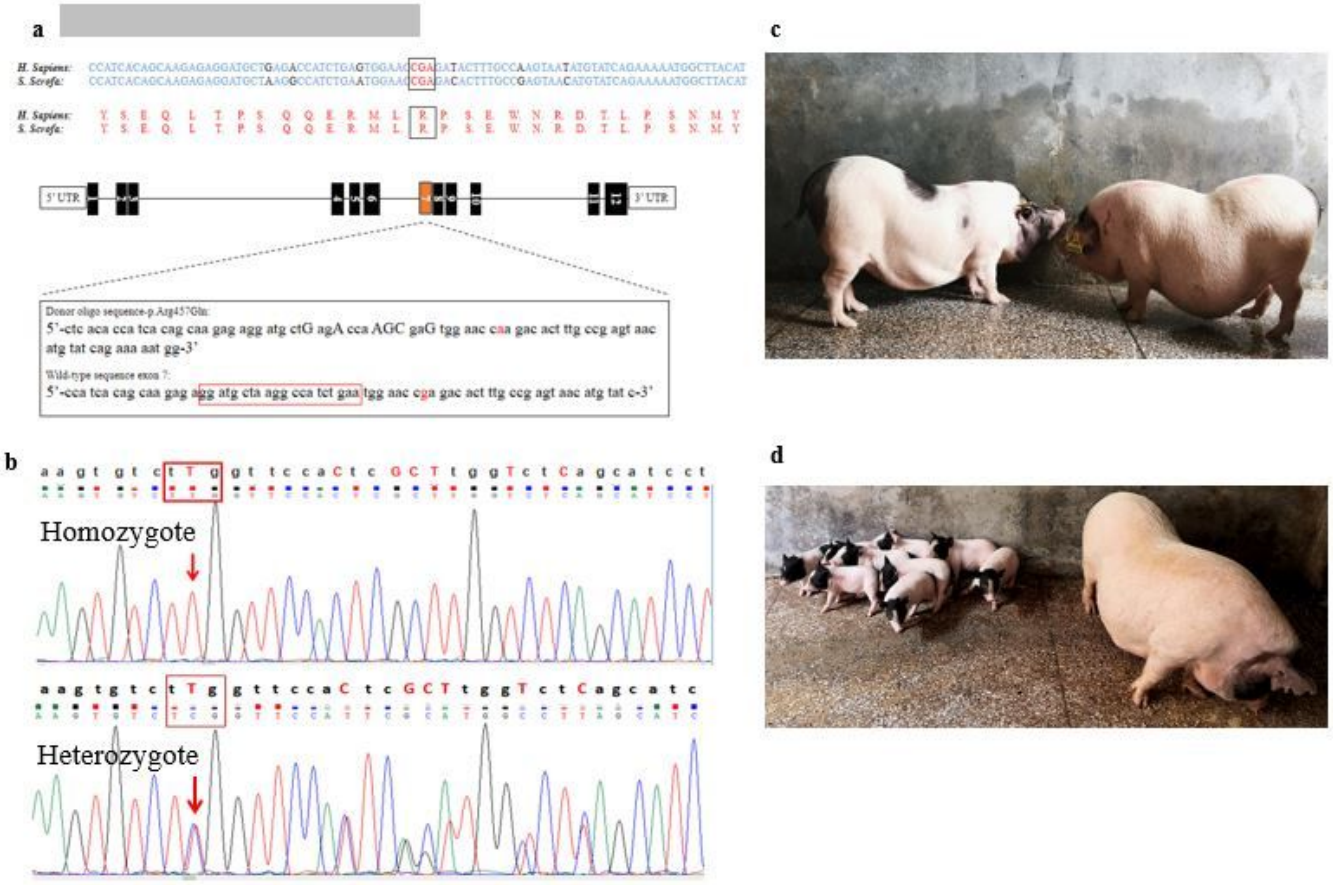


e

| clones | Point mutation number of clones | donor embryos | receptor | CREBRF p.Arg457Gln (F0) | | CREBRF p.Arg457Gln (F1) | | | |
|---|---|---|---|---|---|---|---|---|---|
| | | | | ♂ | ♀ | ♂ | | ♀ | |
| | | | | homozygote | homozygote | homozygote | heterozygote | homozygote | heterozygote |
| 370 | 14 (4.3%) 13, 23, 38, 49, 75, 83, 85, 93, 122, 257, 259, 289, 327, 358 | 843 | 4 | 5 | 7 | 2 | 12 | 5 | 16 |

## Figure 1

CRISPR/Cas9-mediated, HR-independent integration efficiently produced CREBRF p.Arg457Gln pigs and they generated inheritable offsprings. a Schematic representation of the targeting vector. Exons of CREBRF are shown as black boxes, and the orange box in exon 7 represents the sgRNA targeting site, which is enlarged to a rectangle box with the targeting sequence in the red box, the mutated bases in red, and the synonym mutations in capital letters. b Sequencing PCR products of objective DNA fragment

confirmed CREBRFc.1370G>A, p.457Arg>Gln insertion of donor DNA in the cloned pigs. The top one is homozygous CREBRFc.1370G>A, p.457Arg>Gln mutant genotype and the bottom one is heterozygous CREBRFc.1370G>A, p.457Arg>Gln mutant genotype with the bimodal sites being a synonym mutation at the target sites. The red arrow points to the mutation site. c Eight months old wild type(left) and CREBRF p.Arg457Gln mutant F0 pig(right). The CREBRF p.Arg457Gln mutant pig is visibly obese that its belly drags the floor. d The first-generation (F1) pigs (left) at day 15 and their fourteen months old mother pig (CREBRF p.Arg457Gln, F0, right). e CRISPR/Cas9 and ssODN-mediated point mutation in porcine fetal fibroblast cells and generation of CREBRF p.Arg457Gln F0 and F1 p

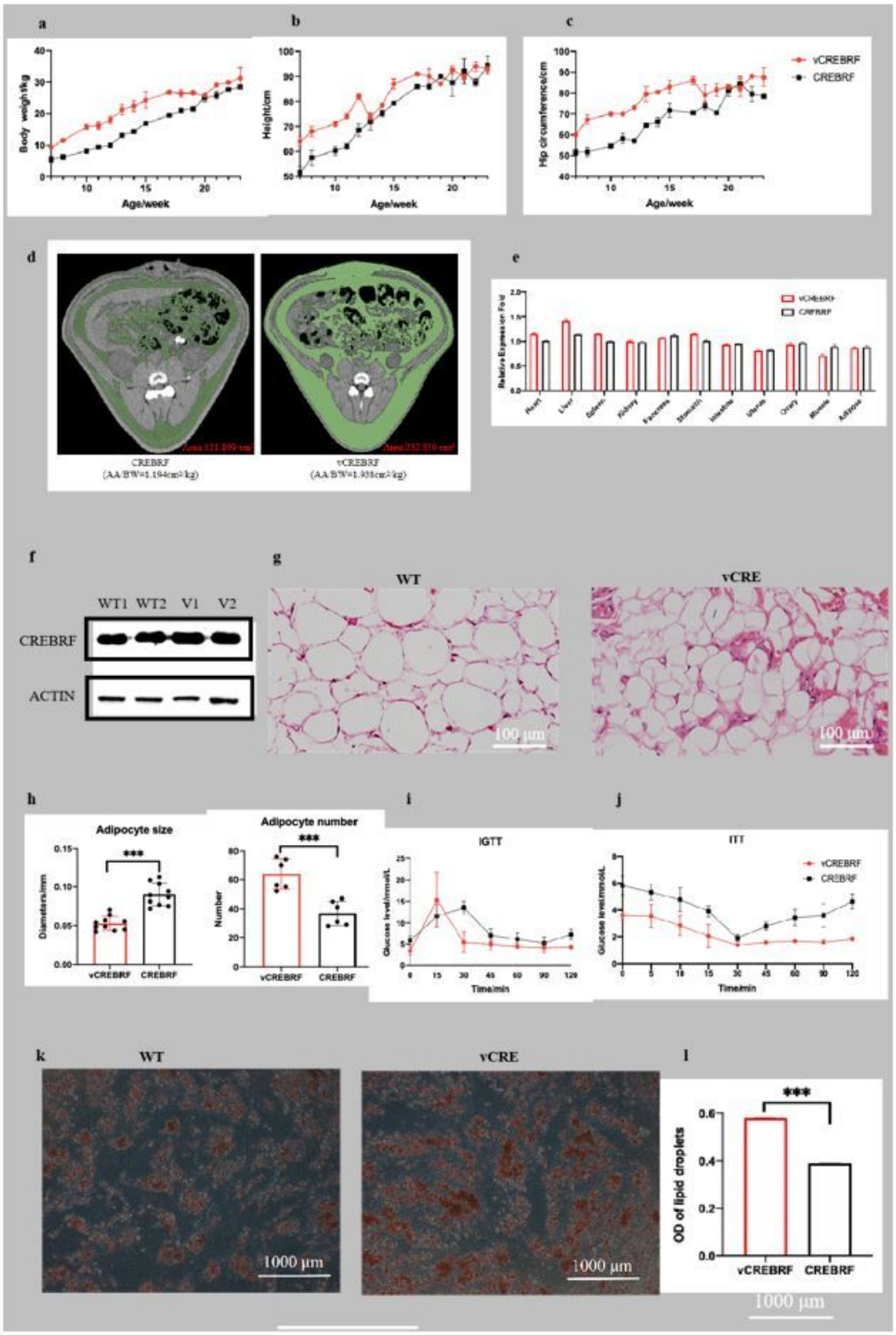


## Figure 2

CREBRF p.Arg457Gln variant pigs increased fat deposition and improved insulin sensitivity. Growth curve from birth to 23 weeks showed that body weight (a) height (b) and hip circumference (c) of CREBRF p.Arg457Gln variant pigs increased compared with that of the WT (n = 4). d CT scanning of 10 weeks old wild-type and CREBRF p.Arg457Gln mutant pigs. The overall abdominal fat mass (green) are calculated between the L3 and L4 of spine. Six pigs, including 3 wild-type female pigs and 3 mutant female pigs,

were scanned respectively. e mRNA expression of CREBRF showed no difference between CREBRF p.Arg457Gln pig and WT pig(both are one year old adult pigs) in tissues including heart, liver, spleen, kidney, pancreas, stomach, intestine, uterus, ovary, musule, adipose .(n=3) f Western blot analysis show no difference of CREBRF expression in WT and CREBRF p.Arg457Gln mutant pigs (one year old adult pigs, n =2). g H&E staining of adipocytes from subcutaneous fat of WT and mutant pigs(one year old adult pigs, n=3). Data showed the adipocytes from mutant pigs is smaller in size and more abundant in number. At least 100 fields of view were observed. (Scale bar: 100 μm.) h The number and diameter of adipocytes in paraffin section (g) under the same field were analyzed statistically. At least 100 fields of view were caculated. i For intravenous glucose tolerance tests(IGTT), pigs were fasted for 16 h, and then challenged with intravenous injection of 50% glucose (1.2 ml/kg body weight). Fasting blood glucose levels are lower at 0 min in p.Arg457Gln variant pigs. Blood glucose level in p.Arg457Gln variant pigs rised rapidly in about 15 minutes, then quickly returned to lower levels than wild type pigs. Pigs are one year old. j For insulin tolerance tests(ITT), pigs were fasted for 12 h and then given an intraperitoneal injection of insulin (0.75 U/kg body weight). After insulin injection, the p.Arg457Gln mutant pigs had lower blood glucose levels than the wild-type ones all the time. Pigs are one year old. (k)&(l) Oil-red-O staining of lipid droplet deposition, which is differentiated from white adipocytes tissue precursor cells deriving from 14-day-old piglets, WT(left), vCREBRF(right). Each the p.Arg457Gln variant group and wild type group were clustered using three piglets respectively. Values are shown as the mean ± SEM; significant differences compared with controls are indicated by **P < 0.001,**P < 0.01 and*P < 0.05. Data were analyzed with a two-sample t test.

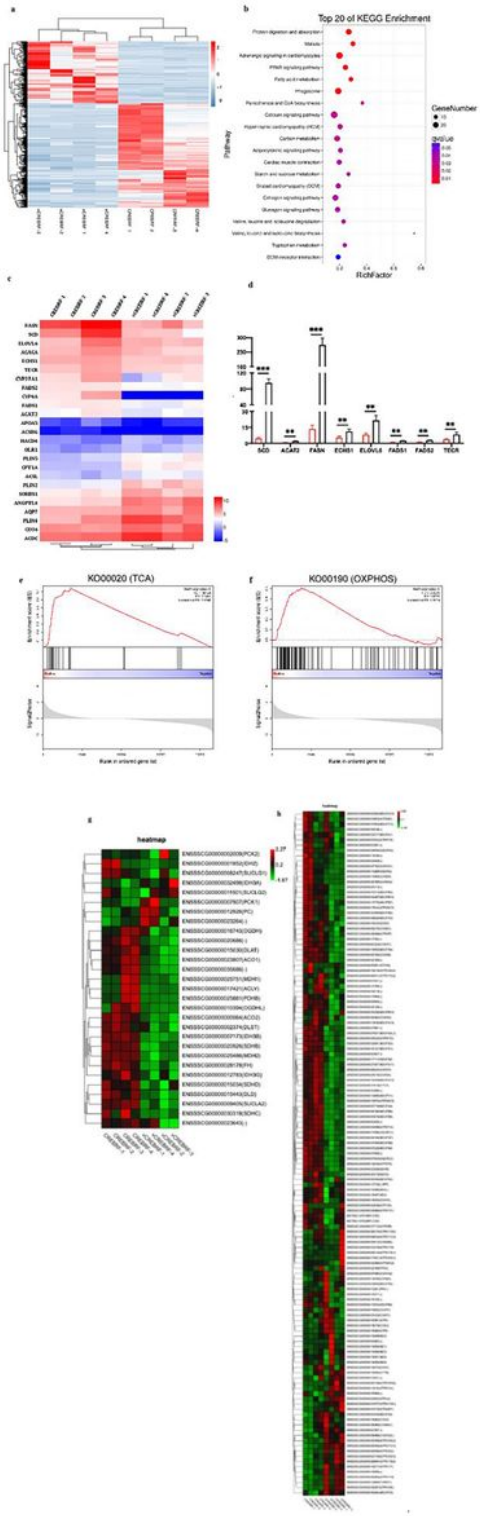


## Figure 3

Identification of DEGs in subcutaneous fat between p.Arg457Gln variant pigs and wild type pigs by RNA-seq. a Heatmap of the expression levels of DEGs. (n=4) b Top 20 KEGG enrichment of the DEGs, c Cluster analysis of DEGs in lipid synthesis and fatty acid transport. d Q-PCR results of fatty acid synthesis-related genes. e Profile of the running ES score & positions of Gene set member on the TCA list by GSEA. f Profile of the running ES score & positions of Gene set member on the OXPHOS list by GSEA. g Profile of

DEGs expression levels in TCA enplot. h Profile of DEGs expression levels in OXPHOS enplot. DEGs: differentially expressed genes. KEGG: Kyoto Encyclopedia of Genes and Genomes. TCA: Citrate Cycle. OXPHOX: Oxidative phosphorylation. GSEA: Gene set enrichment analysis. Each the p.Arg457Gln variant group and wildtype group were clustered using four healthy adult pigs(more than one year old), respectively. Significant difference was assessed by p<0.05, FDR-adjusted.

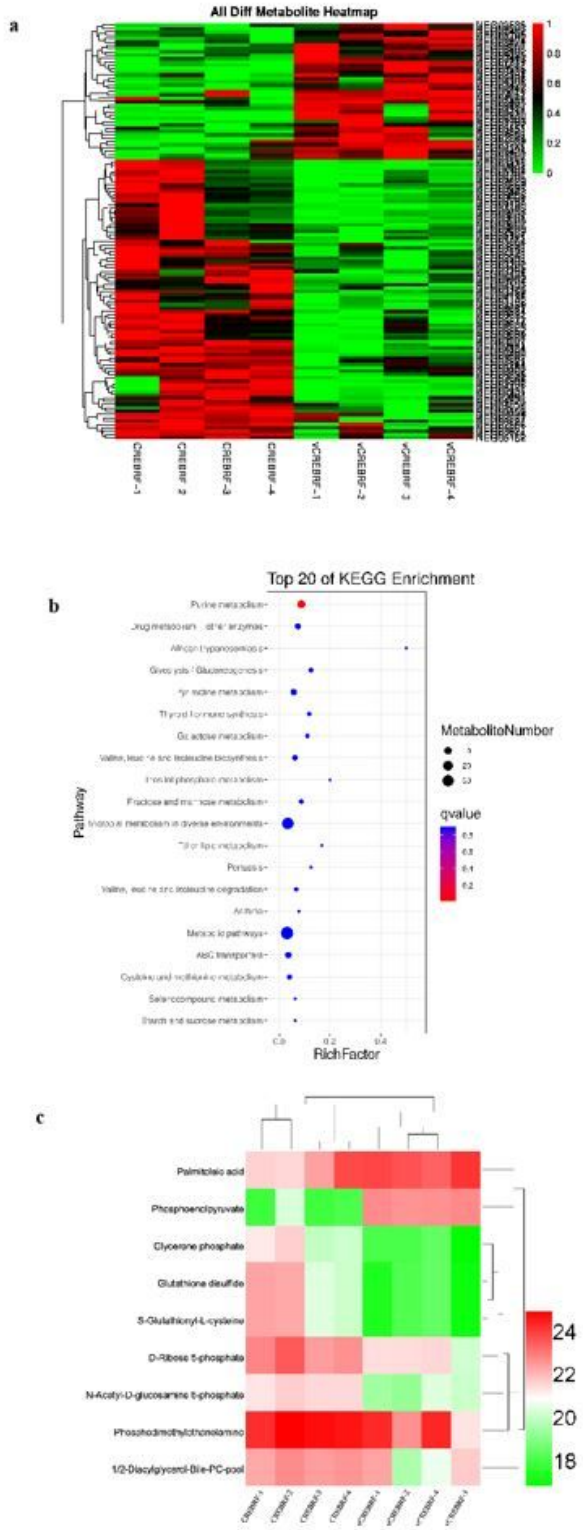


## Figure 4

Identification of differential metabolites in subcutaneous fat between p.Arg457Gln variant pigs and wildtype pigs by untargeted metabolome analysis. a Heatmap of the contents of differential metabolites. b Top 20 KEGG enrichment of the differential metabolites. c Cluster analysis of differential metabolites related to Glycolysis, Lipogenesis and Pre-oxidative metabolic processes. P□0.05 and VIP≥1 were considered differential metabolites between these two groups.

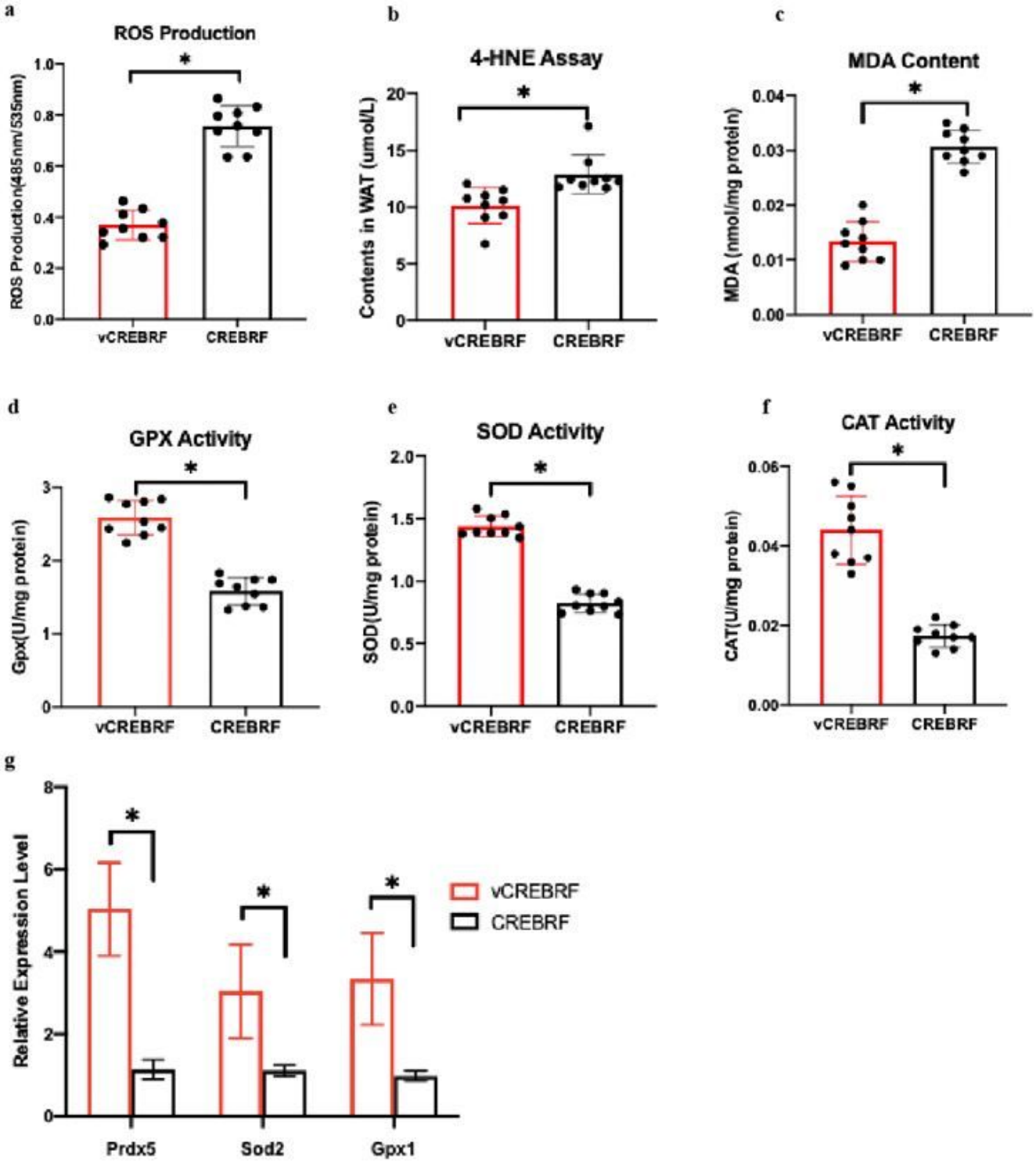


Figure 5

Detection of lipid peroxidation level in subcutaneous fat between p.Arg457Gln variant pigs and wildtype pigs. a ROS production. b 4-HNE content. c MDA content. d GPX activity. e SOD activity. f CAT activity. g RNA expression level of Prdx5, Sod2 and Gpx1. Data are mean ± sem of biologically independent samples. *P<0.05; **P<0.01;***P<0.001.

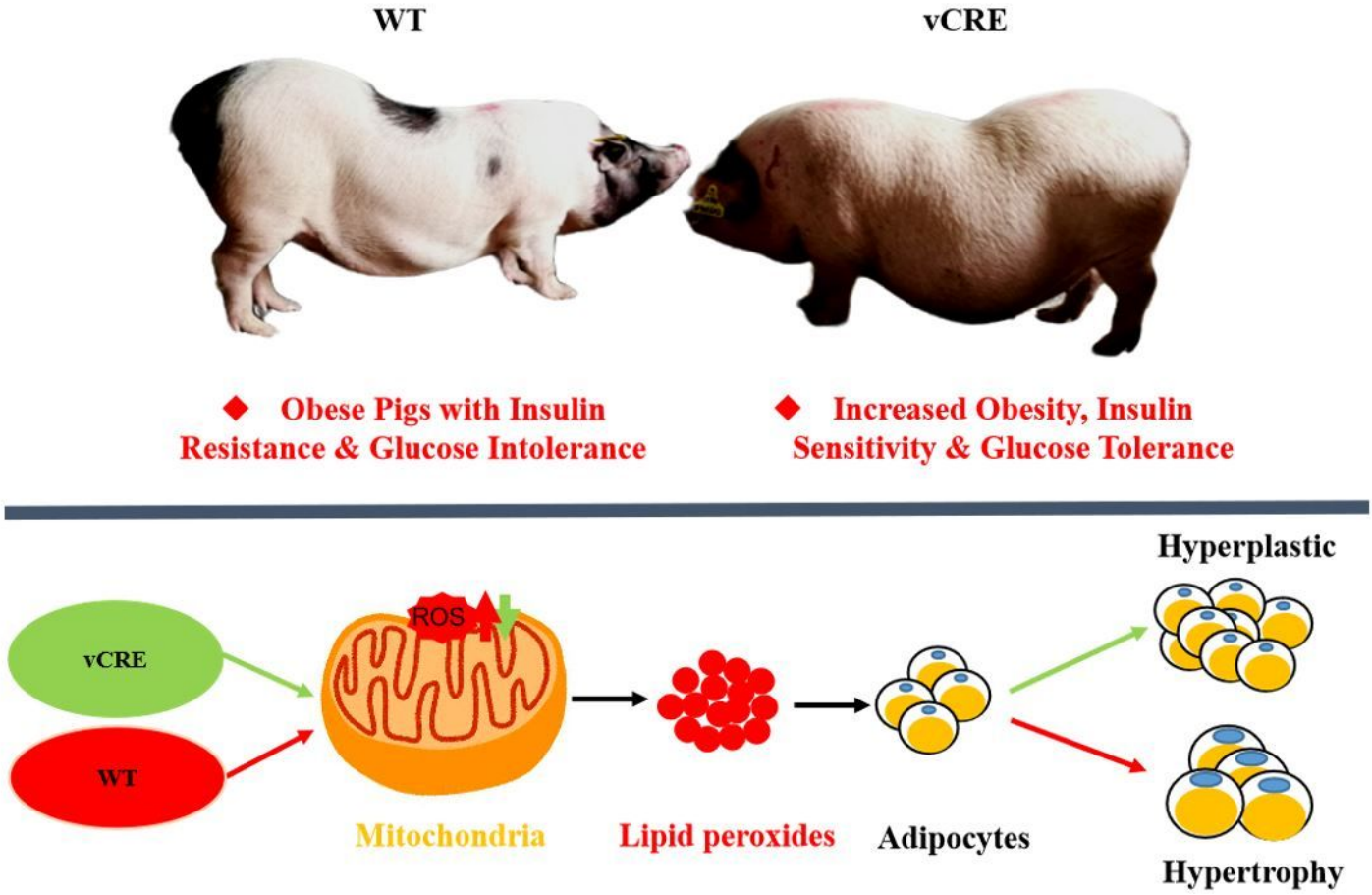


**Figure 6**

Illustration summarizing the metabolism-related role of CREBRF-p.Arg457Gln variant in the mitochondria of adipocytes under obese conditions. CREBRF p.Arg457Gln variant promotes the generation of adipocyte to increase energy storage and reduces the production of ROS by reducing oxidation capacity, which protects the body from lipid peroxidation and reduces insulin resistance.

## Supplementary Files

This is a list of supplementary files associated with this preprint. Click to download.

- SuppFile.docx